Available online at www.sciencedirect.com
ScienceDirect
Proceedings of the Combustion Institute 32 (2009) 769–775
Proceedings of the Combustion Institute
www.elsevier.com/locate/proci

Soot formation and temperature field structure in co-flow laminar methane–air diffusion flames at pressures from 10 to 60 atm

Hyun I. Joo, Ömer L. Gülder *

Institute for Aerospace Studies, University of Toronto, 4925 Dufferin Street, Toronto, Ont., Canada M3H 5T6

Abstract

The effects of pressure on soot formation and the structure of the temperature field were studied in co-flow methane–air laminar diffusion flames over a wide pressure range, from 10 to 60 atm in a high-pressure combustion chamber. The selected fuel mass flow rate provided diffusion flames in which the soot was completely oxidized within the visible flame envelope and the flame was stable at all pressures considered. The spatially resolved soot volume fraction and soot temperature were measured by spectral soot emission as a function of pressure. The visible (luminous) flame height remained almost unchanged from 10 to 100 atm. Peak soot concentrations showed a strong dependence on pressure at relatively lower pressures; but this dependence got weaker as the pressure is increased. The maximum conversion of the fuel's carbon to soot, 12.6%, was observed at 60 atm at approximately the mid-height of the flame. Radial temperature gradients within the flame increased with pressure and decreased with flame height above the burner rim. Higher radial temperature gradients near the burner exit at higher pressures mean that the thermal diffusion from the hot regions of the flame towards the flame centerline is enhanced. This leads to higher fuel pyrolysis rates causing accelerated soot nucleation and growth as the pressure increases.

Keywords: Soot formation; High-pressure combustion; Methane–air diffusion flames; Soot and temperature measurements

1. Introduction

Soot emissions resulting from diffusive combustion of hydrocarbons have long been recognized as a significant problem. For example, the presence of soot affects adversely the performance of propulsion systems. Continuum radiation from soot is the dominant mechanism of the spread of unwanted fires. Soot radiation is the major heat load on combustor components causing maintenance and reliability problems. Soot itself is intrinsically toxic and soot particles are strongly associated with detrimental health effects. In the earth's atmosphere soot contributes to the entrapment of the solar radiation that is believed to lead to global warming. Further, when soot aerosols are deposited on ice and snow covered surfaces, they reduce the sea ice and snow albedo leading to higher heat absorbtion [1,2]. It is suggested that reducing soot emissions, and thereby restoring snow albedos to pristine high values would in turn have the effect of reducing global warming [1].

* Corresponding author. Fax: +1 416 667 7799.
E-mail address: ogulder@utias.utoronto.ca (Ö.L. Gülder).

1540-7489/$ - see front matter © 2009 The Combustion Institute. Published by Elsevier Inc. All rights reserved.
doi:10.1016/j.proci.2008.06.166

Soot formation and oxidation in combustion devices are dependent on several parameters. One of the most important of these is the pressure which has a significant influence on the rate of soot formation and oxidation in combustion systems. Although most of the practical combustion devices used in transportation systems and stationary gas turbine combustors operate at elevated pressures, our understanding of the effects of pressure on soot formation and oxidation processes is limited. In most practical diffusion combustion systems and fires, the combustion is turbulent. However, the high level of intermittency and short residence times involved in these flames are not always suitable for direct experimental studies of combustion events like soot formation. One of the most widely used approximations is to exploit the similarities in laminar and turbulent diffusion flames using approaches like the laminar flamelet concept that facilitates a tractable flame model. For this reason, most of the soot measurements are made in laminar diffusion flames that provide easily controlled conditions and the results can be projected to practical turbulent flames.

Current understanding of the influence of pressure on soot formation and oxidation is limited. Flower and Bowman [3] studied laminar diffusion flames of ethylene at a pressure range of 1–10 atm, by measuring line-of-sight integrated soot volume fractions and temperatures along the flame centerline. They report a pressure scaling of maximum integrated soot volume fraction with an exponent of 1.2 from atmospheric to 10 atm pressure for ethylene diffusion flames. Measurements of Lee and Na [4] indicate a similar pressure scaling for the maximum integrated soot volume fraction with an exponent of 1.26 in laminar ethylene flames from atmospheric to 4 atm. Lee and Na [4] also report limited radially resolved soot volume fraction data that imply a square dependence on pressure of maximum local soot volume fraction at a height of 20 mm above the burner rim. McCrain and Roberts [5] measured path integrated and local soot volume fractions by line-of-sight attenuation and laser-induced incandescence, respectively. Their measurements covered a pressure range of 1–25 atm in methane flames and 1–16 atm in ethylene diffusion flames yielding similar pressure exponents as [3,4]. Thomson et al. [6] reported radially resolved soot concentration and soot temperature results in laminar diffusion flames of methane using soot emission spectroscopy and line-of-sight attenuation which are the first detailed measurements of soot and temperature done at elevated pressures up to 40 atm. It was shown that in high-pressure laminar diffusion flames, fraction of fuel's carbon content that is converted to soot, rather than the line-of-sight integrated volume fraction, should be used in assessing the sensitivity of soot formation to pressure [3,6]. Measurements by Bento et al. [7] on laminar diffusion flames of propane covered the pressure range from atmospheric to 7.2 atm and their results were comparable to [6] for the low pressure range.

The main objective of the research reported in this paper is to extend the measurements reported in [6] beyond 40 atm and determine spatially resolved soot volume fraction and temperature in methane diffusion flames at elevated pressures. Spectral soot emission (SSE) measurements in the methane flame are presented for pressures from 10 to 60 atm.

2. Experimental methodology

The experimental high-pressure combustion chamber and the laminar diffusion flame burner used in this study are described in detail in [6,7]. The design pressure of the chamber is about 110 atm, and its internal diameter and internal height are 0.24 and 0.6 m, respectively. Optical access into the chamber is through three ports at 0°, 90°, and 180° locations allowing line-of-sight measurements as well as 90° scattering and imaging experiments. The burner has a fuel nozzle exit diameter of 3.06 mm and an air nozzle diameter of 25 mm. Sintered metal foam elements are included in the fuel and air nozzles to straighten and reduce the instabilities in the flow and to create a top hat exit velocity profile as the gases leave the foam elements. A schematic of the vessel is shown in Fig. 1.

The theory and overall experimental layout of the spectral soot emission diagnostic (SSE) are described previously [6–8]. In SSE, line-of-sight radiation emission from soot is measured along chords through the flame. A series of emission projections at a given height in the flame can be inverted to obtain radially resolved

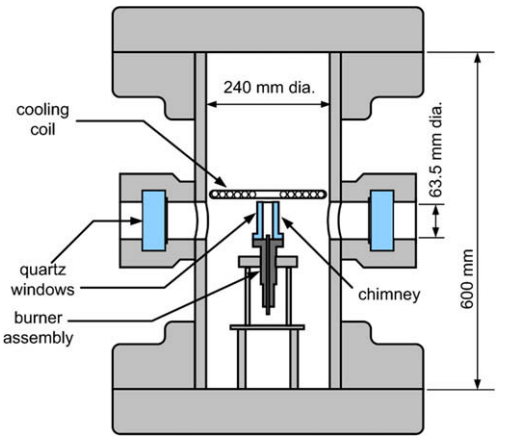

Fig. 1. A schematic of the high-pressure combustion chamber.

emission rates from which temperature and soot volume fraction can be determined when soot optical properties are known [9]. The emitted radiation from soot first passes through an adjustable aperture and lens unit. For the current study an aperture diameter of approximately 6.2 mm and associated f-number of $f/48$ was used. The lens selected for this study is an achromatic doublet lens with a focal length of 300 mm. The lens has an antireflective coating, effective within the wavelength range of 650–1050 nm. The purpose of the lens is to image the flame radiation onto the entrance slit of the spectrometer. The lens is positioned to produce a 1:1 image with no magnification. The entrance to the spectrometer contains two slits: the vertical slit is approximately 25 μm in width and the horizontal slit is approximately 290 μm in height. The slit sizes play a role in the resulting spatial resolution of the collected data.

The spectrometer is an imaging Czerny–Turner spectrometer that internally uses aspheric mirrors. The spectrometer grating used for this task has a blaze wavelength of 750 nm and is manufactured with 300 groves/mm. The spectrometer has a dispersion of approximately 18.84 nm/mm.

The total array size of the CCD is 1340×400 pixels. However, due to the restricted size of the entrance slit, a region of interest of size 1340×80 pixels was selected. Combined with the previously mentioned spectrometer and grating, the CCD camera is capable of capturing an approximate wavelength spread of 505 nm across the camera array, providing a spectral step size of 0.377 nm/pixel. However, the CCD resolution at FWHM (full width at half maximum) using 2.5 pixels, is approximately 0.942 nm. The exposure time is controlled by an electronic shutter mounted on the front face of the camera, just forward of the CCD array. The shutter speed was selected based on an optimal intensity count registered on the CCD. After viewing the methane–air diffusion flame at various pressures, an exposure time of one second was selected. Knife edge scans were performed to locate the focal point as well as to determine that an appropriate depth of field had been met. The spatial resolution of the SSE system was also determined through the analysis of knife edge scans. The horizontal spatial resolution was found to be approximately 70 μm. The vertical spatial resolution was inferred to be approximately 290 μm. In order to calibrate the spectral axis of the CCD array a pencil style neon calibration lamp was used. The system is calibrated for radiation intensity using a filament lamp, with a calibration traceable to NIST, placed inside the chamber. The uncertainty in the spectral radiance temperature is about 5 K. Further details of the experimental set-up and data reduction are given in [6–8].

The fuel flow rate was selected to match the carbon mass flow rate of the studies performed previously with methane diffusion flames up to 40 atm [6], and propane diffusion flames up to 7.2 atm [7]. A constant methane mass flow rate of 0.55 mg/s, which corresponds to a carbon mass flow rate of 0.412 mg/s, was maintained at all pressures. For each pressure, measurements were obtained at height increments of 0.5 mm from the burner tip to the tip of the flame and at horizontal increments of 50 μm.

3. Results and discussion

As the pressure was increased, axial flame diameters decreased giving an overall stretched appearance to the flame as noted by Flower and Bowman [3], Thomson et al. [6] and Bento et al. [7]. For pressures between 10 and 60 atm, the flame radius varied by approximately, $r_f \propto P^{-0.5}$ and the flame cross-sectional area varied by approximately, $A_f \propto P^{-1}$. This observation is in agreement with previous experimental results using methane and propane flames [5–7]. An inverse dependence on pressure for the flame cross-sectional area implies that residence times are independent of pressure which allows measurements to be compared at the same height above the burner exit. This has also been confirmed by a recent numerical effort [10] that shows that the axial velocity profiles are pressure independent along the flame centerline in methane diffusion flames between 5 and 40 atm.

This can also be illustrated by using the flame height expressions developed in [11]. It is shown that, to a first approximation, the height of a buoyancy-dominated laminar co-flow diffusion flame, established on a circular fuel nozzle, scales with molecular diffusivity, D, and fuel flow rate, Q, as [11],

$$H \propto \frac{Q}{D} \propto \frac{1}{P}\frac{vA}{D}, \tag{1}$$

for a fixed flow rate of fuel. Here, v is the mean fuel exit velocity and A is the fuel nozzle exit area. Since molecular diffusivity, D, is inversely proportional to pressure, P (i.e. $D \propto 1/P$), then the height of the diffusion flame is independent of the pressure. At a given height above the burner nozzle exit, the average velocity within the flame envelope will not change with pressure, if the flame cross-sectional area varies inversely with pressure. That is, as the pressure increases, the material flow within the flame envelope will be through a narrower cross-section but at a higher density, thus keeping the average velocity constant at a given height.

Visible flame heights, as indicated by soot radiation, remained constant at approximately 9 mm between pressures 10 and 100 atm. For pressures

lower than 10 atm, visible flame heights tended to decrease and the blue flame region near the nozzle exit became more expansive as the pressure neared atmospheric pressure. Soot formation seemed to occur mainly at the tip of the flame for lower pressures, however, as the pressure increased, the luminous carbon zone moved downward filling an increasingly larger portion of the flame. Similar observations were reported for ethane and propane diffusion flames [7,12]. In [6], soot volume fraction and temperature profiles throughout the methane diffusion flame were reported as a function of pressure between 0.5 and 4 MPa at a constant methane mass flow rate of 0.55 mg/s. Also reported were the methane diffusion flame pictures at various pressures at a constant methane mass flow rate of 0.66 mg/s. These pictures depicted an almost constant visible flame height between 5 and 20 atm. But the visible flame height started getting shorter as the pressure increased further up to 80 atm. The gradual reduction in visible flame height with pressure beyond 20 atm could not be replicated through several repeat measurements – in all experimental sets the visible flame height remained constant between 10 and 100 atm.

A three-dimensional depiction of the soot volume fraction as a function of pressure, and spatial location within the flame is shown in Fig. 2. Soot volume fraction increases significantly with increasing pressure and the maximum soot location moves towards the centerline. Detailed radial soot concentration profiles in methane diffusion flames are shown in Figs. 3–8 at heights of 0.5–9 mm above the burner rim at 40, 50, and 60 atm. Measurements were made by scanning the entire flame diameter at each measurement height; however, the data shown in Figs. 2–8 represent averages of the left and right side scans.

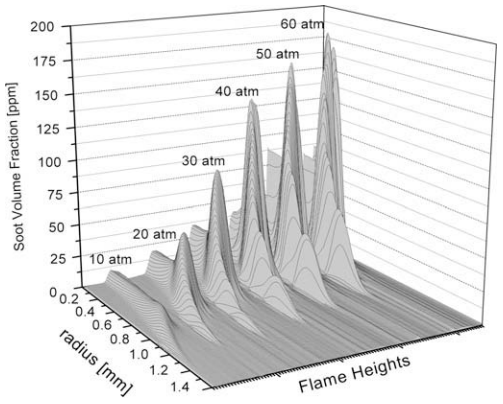

Fig. 2. A three-dimensional rendition of the soot volume fraction as a function of pressure and the spatial location within the flame. It should be noted that the "Flame Heights" coordinate is successive flame heights, from the burner rim to the tip of the flame, for each flame at various pressures as indicated.

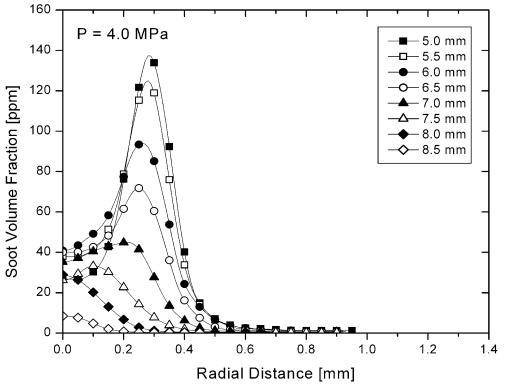

Fig. 4. Soot concentration profiles at 40 atm at the upper half of the flame, from 5 to 8.5 mm above the burner rim.

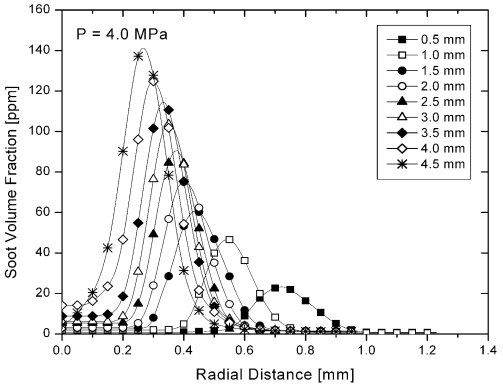

Fig. 3. Soot concentration profiles at 40 atm at the lower half of the flame, from 0.5 to 4.5 mm above the burner rim.

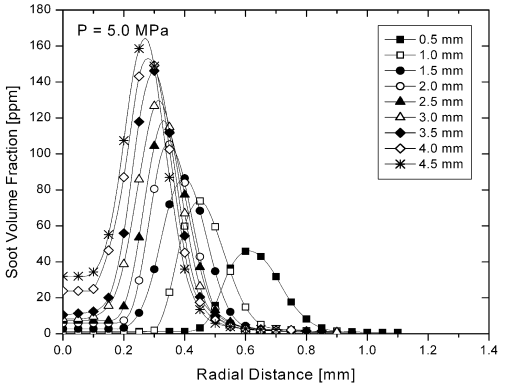

Fig. 5. Soot concentration profiles at 50 atm at the lower half of the flame, from 0.5 to 4.5 mm above the burner rim.

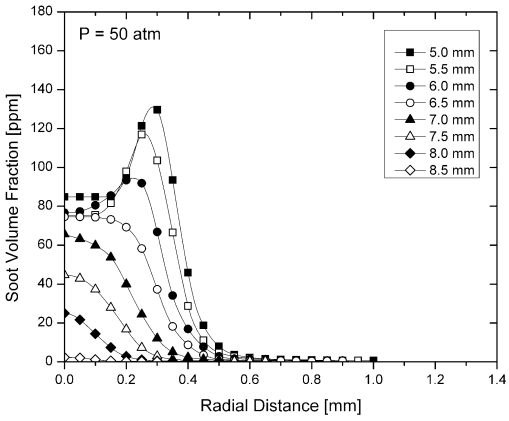

Fig. 6. Soot concentration profiles at 50 atm at the upper half of the flame, from 5 to 8.5 mm above the burner rim.

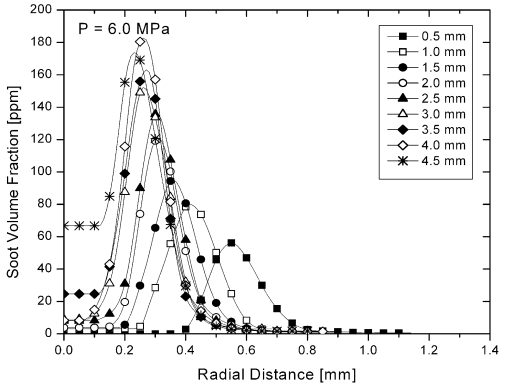

Fig. 7. Soot concentration profiles at 60 atm at the lower half of the flame, from 0.5 to 4.5 mm above the burner rim.

Soot forms first in an annular band near the burner rim, much like the atmospheric laminar diffusion flames. Near the mid height of the flame, the annular distribution of soot remains pronounced, but soot also begins to appear in the core of the flame. Soot appearance in the core of the flame at lower flame heights occurs at higher pressures, see, e.g., Figs. 5 and 7. At the tip of the flame, the annular distribution disappears and a peak soot concentration is observed on the flame centerline. The contraction of the flame diameter with pressure is reflected in the location of the peaks in the radial profiles of soot volume fraction, Fig. 2. Soot concentrations showed a significant increase with pressure; the peak soot volume fraction increased from about 14 ppm at 10 atm to over 180 ppm at 60 atm.

As expected, soot volume fraction increases with increasing pressure since the flame is narrowing which suggests that all species are at higher concentrations. Further, the enhanced air entrainment with pressure into the flame near the burner rim is expected to accelerate the pyrolysis process [10]. To assess the sensitivity of sooting propensity of the flame to pressure, previous studies suggested [3,6,7] that the percentage of total carbon in the fuel converted to soot as a function of height is a better measure than the maximum line-of-sight integrated soot concentrations. We use the same approach here to assess the influence of pressure. The mass flow rate of carbon, in the form of soot, can be determined through the relationship

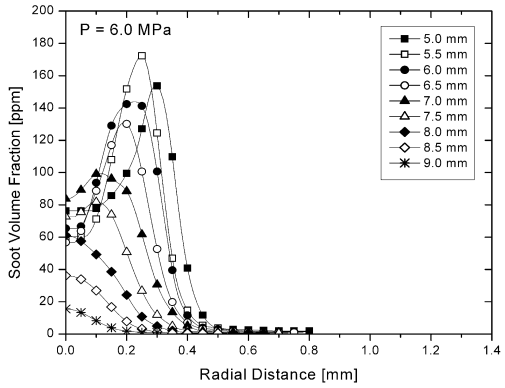

Fig. 8. Soot concentration profiles at 60 atm at the upper half of the flame, from 5 to 9 mm above the burner rim.

$$\dot{m}_s(z) = v_z(z)\rho_s \int 2\pi r f_v(r,z)\,dr, \tag{2}$$

where v_z is the axial velocity, $\rho_s = 1.8$ g/cm^3 is the soot density, and z is the axial height. The axial velocity is estimated using the relationship, $v_z(z) = \sqrt{2az}$, where a is an acceleration constant commonly assumed to be 25 m/s^2 [3,13]. The percentage of carbon in the fuel converted to soot is simply $\eta_s = \dot{m}_s/\dot{m}_c$, where $\dot{m}_c$ is the carbon mass flow rate at the nozzle exit. A plot of maximum percentage conversion of carbon to soot as a function of pressure is shown in Fig. 9 as a logarithmic plot. However, a single power-law relationship between the percentage conversion of fuel's carbon to soot and the pressure is not obvious. The pressure sensitivity decreases significantly as pressure is increased. Also shown in Fig. 9 are the data reported in [6] for methane flames with identical experimental setup and conditions for the pressure range of 5 to 40 atm. Agreement is within the experimental error margins except at 40 atm. For a power-law relationship of $\eta_s \propto P^n$, n is about 0.33 between 30 and 60 atm for the present data. In [6], it was reported as 0.1 between 20 and 40 atm. Lower soot concentrations at 40 atm observed in [6] is more likely related to the decreasing flame heights with pressure. It is suspected that in [6] above 20 atm the mass flow rate of

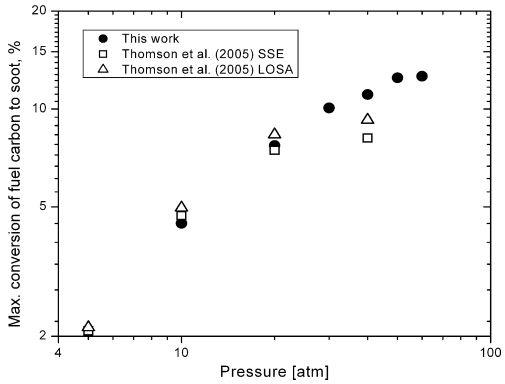

Fig. 9. Maximum conversion of fuel's carbon to soot as a function of pressure. In the legend, SSE refers to soot spectral emission and LOSA to line-of-sight attenuation techniques.

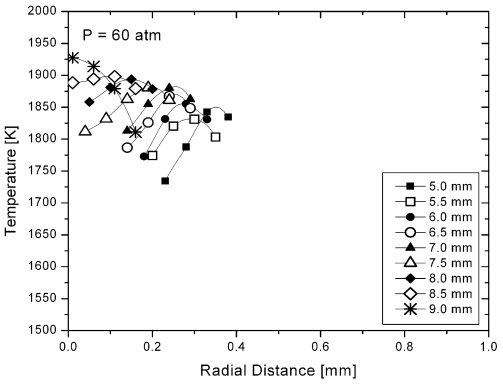

Fig. 11. Radial temperature profiles at 60 atm at the upper part of the flame from 5 to 9 mm.

the fuel was not constant but was gradually decreasing with pressure due to difficulties in calibration of mass flow-meters operating at high pressures.

Representative soot temperature profiles are shown in Figs. 10 and 11 at various heights above the burner exit at 60 atm. Since the spectral soot emission technique used in this study is based on measurements of soot emission, temperatures can only be determined in locations where sufficient soot exists to provide a resolvable signal. These regions typically occur at radial locations centered about the zones of peak soot volume fraction. From previous characterization of the SSE diagnostic [8], temperatures are known to decrease at the outer edges of the annuli earlier than would be predicted by flame models or other experimental diagnostics, thus under-predicting the peak temperature in the reaction zone. It is believed that this fall off is caused by errors introduced through the inversion algorithm when inverting the rapidly decreasing line-of-sight emission intensities at the edge of the flame. In the core of the flame, temperatures can also be inaccurate due to low soot volume fractions relative to peak soot volume fractions in the annulus [6]. It is possible that the increased uncertainties of temperatures in the core of the flame and on the outside of the soot annulus may be linked to optical limitations and beam steering when the current temperature diagnostic is applied in such a narrow flame. Consequently, the temperature plots provided here have been limited to regions centered about the soot annuli. The radial temperature profiles are similar to those observed in high-pressure diffusion flames of methane and propane [6,7]. Multiple measurements at the same location on different occasions showed that the temperature curves are repeatable, within 2%, including any anomalous temperature values discussed above.

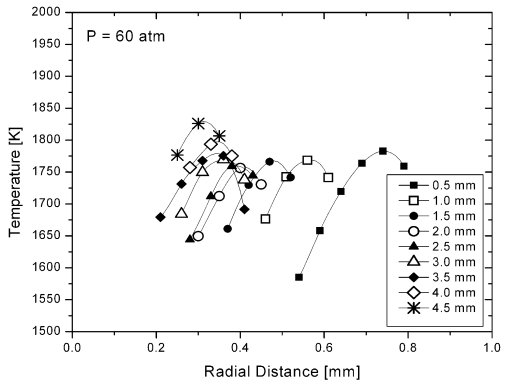

Fig. 10. Radial temperature profiles at 60 atm at the lower part of the flame from 0.5 to 4.5 mm.

As the pressure increases, the visible flame gets narrower resulting in steeper radial temperature gradients. Maximum radial temperature gradients, calculated from the temperature profiles, are shown in Fig. 12. The gradients are highest near the burner rim, and generally decrease with increasing height. The radial temperature gradients generally increase with pressure at very low heights and near the tip of the flame. Near the burner nozzle, radial temperature gradients are as high as 1600 K/mm at the higher pressures, whereas they drop to about 0 near the tip of the flame, Fig. 12. Higher radial temperature gradients near the burner exit at higher pressures mean that the thermal diffusion from the hot regions of the flame towards the flame centerline is enhanced. This causes higher fuel pyrolysis rates which lead to accelerated soot nucleation and growth as the pressure increases.

Modelling of the flame emission using the methods described in [8] showed that attenuation of emission by soot introduces only a small error in the measurements (i.e. <2%) for even the high-

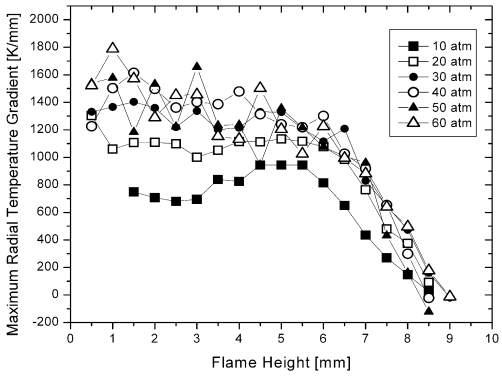

Fig. 12. Maximum radial temperature gradient at various pressures as a function of the height above the burner rim.

est soot loadings observed in this flame. This result may seem surprising considering that soot volume fractions of 180 ppm have been measured in this flame; however, light attenuation is a function of the product of the soot concentration and the absorption path length. Although soot concentrations are a factor of 10 larger than those observed in the familiar atmospheric flames, e.g. [14,15], the flame diameter is much smaller and decreases with increasing pressure. A more detailed discussion of the subject can be found in [16]. Potential errors introduced in soot concentration and temperature measurements due to the uncertainty in soot refractive index are discussed in detail in [6].

4. Concluding remarks

Soot volume fraction and soot temperature profiles were measured using spectral soot emission to study the sensitivity of soot formation to pressure in coflow laminar diffusion flames of methane in air in a high-pressure combustion vessel. The range of pressures investigated was from 10 to 60 atm. The mass flow rate of the methane was kept constant at all pressures. Visible flame heights, as indicated by soot radiation, remained constant at approximately 9 mm between 10 and 100 atm. For pressures lower than 10 atm, visible flame heights decreased with decreasing pressure. Between 10 and 60 atm, the cross-sectional area of the flame (measured from the radius defined by either the maximum soot or maximum temperature annuli) showed an inverse dependence on pressure. Peak carbon conversion to soot, defined as the percentage of the fuel's carbon content converted to soot, showed a strong pressure dependence at relatively lower pressures; as the pressure is further increased this dependence got weaker. The maximum conversion of the fuel's carbon to soot, 12.6%, was observed at 60 atm at approximately the mid-height of the flame. Radial temperature gradients within the flame increased with pressure and decreased with flame height above the burner rim. Higher radial temperature gradients near the burner exit at higher pressures mean that the thermal diffusion from the hot regions of the flame towards the flame centerline is enhanced. This leads to higher fuel pyrolysis rates causing accelerated soot nucleation and growth as the pressure increases.

Acknowledgments

We acknowledge an infrastructure grant provided by Canadian Foundation for Innovation (CFI) for building the high-pressure combustion vessel and associated components as well as acquiring the diagnostic equipment. Operational funds for this work has been provided by Natural Sciences and Engineering Research Council (NSERC), Canadian Space Agency (CSA), and AUTO 21.

References

[1] J. Hansen, L. Nazarenko, *Proc. Natl. Acad. Sci. USA* 101 (2004) 423–428.
[2] Y. Kim, H. Hatsushika, R.R. Muskett, K. Yamazaki, *Atmos. Environ.* 39 (2005) 3513–3520.
[3] W.L. Flower, C.T. Bowman, *Proc. Combust. Inst.* 21 (1988) 1115–1124.
[4] W. Lee, Y.D. Na, *JSME Int. J. Ser. B* 43 (4) (2000) 550–555.
[5] L.L. McCrain, W.L. Roberts, *Combust. Flame* 140 (2005) 60–69.
[6] K.A. Thomson, Ö.L. Gülder, E.J. Weckman, R.A. Fraser, G.J. Smallwood, D.R. Snelling, *Combust. Flame* 140 (2005) 222–232.
[7] D.S. Bento, K.A. Thomson, Ö.L. Gülder, *Combust. Flame* 145 (2006) 765–778.
[8] D.R. Snelling, K.A. Thomson, G.J. Smallwood, Ö.L. Gülder, E.J. Weckman, R.A. Fraser, *AIAA J.* 40 (9) (2002) 1789–1795.
[9] C.J. Dasch, *Appl. Opt.* 31 (8) (1992) 1146–1152.
[10] F. Liu, K.A. Thomson, H. Guo, G.J. Smallwood, *Combust. Flame* 146 (2006) 456–471.
[11] F.G. Roper, C. Smith, A.C. Cunningham, *Combust. Flame* 29 (3) (1977) 227–234.
[12] P.M. Mandatori, *Soot Formation in Ethane–Air Coflow Diffusion Flames at Elevated Pressures*, MASc thesis, Institute for Aerospace Studies, University of Toronto, Canada, 2006.
[13] F.G. Roper, *Combust. Flame* 29 (3) (1977) 219–226.
[14] D.R. Snelling, K.A. Thomson, G.J. Smallwood, Ö.L. Gülder, *Appl. Opt.* 38 (12) (1999) 2478–2485.
[15] R.J. Santoro, T.T. Yeh, J.J. Horvath, H.G. Semerjian, *Combust. Sci. Technol.* 53 (2–3) (1987) 89–115.
[16] J.J. Murphy, C.R. Shaddix, *Combust. Flame* 143 (2005) 1–10.